Effects of quenched disorder on the orientational order of the octylcyanobiphenyl liquid crystal

Huairen Zeng,[1] Bostjan Zalar,[2] Germano S. Iannacchione,[3] and Daniele Finotello[1]
[1]*Department of Physics, Kent State University, Kent, Ohio 44242*
[2]*Jozef Stefan Institute, University of Ljubljana, Jamova 39, 1000 Ljubljana, Slovenia*
[3]*Department of Physics, Worcester Polytechnic Institute, Worcester, Massachusetts 01609*
(Received 18 June 1999)

Deuteron NMR (DNMR) measurements were performed with high-temperature and spectral resolution on the octylcyanobiphenyl (8CB) liquid crystal confined to the randomly interconnected pores of silica aerogel as a function of temperature and silica density. The aerogel density was varied by one order of magnitude and the temperature spanned the isotropic (*I*), nematic (*N*), and smectic-*A* (Sm*A*) phases of 8CB. For all samples, the liquid crystal was confined to pores smaller than the micron-sized magnetic coherence length. Thus the observed line shapes reflect the director pattern, $\hat{n}(\vec{r})$, and the orientational order, *Q*, as dictated by the porous host. The DNMR spectral patterns are consistent with powder line shapes representative of a randomized $\hat{n}(\vec{r})$ characterized by a single *Q*. The nematic domains formed are of finite dimension that likely exceeds the confining size. The weakly first-order nematic-to-isotropic phase transition becomes less discontinuous with decreasing pore size, eventually becoming continuous at an aerogel density between 0.36 and 0.5 g/cm^3. In the most severe confinement, no phase transitions are observed with only a continuous evolution of *Q* present. The orientational order is suppressed from the bulk's with no enhancement upon the onset of the Sm*A* phase. This indicates a decoupling of nematic and smectic order parameters and a severe suppression of the Sm*A* phase by this porous media. [S1063-651X(99)08711-5]

PACS number(s): 61.30.−v, 65.20.+w, 76.60.−k

I. INTRODUCTION

The study of physical systems constrained to hosts composed of a random network of pores has led to a variety of unexpected, interesting, and complex phenomena. Fundamental questions of how the phase structure or phase transitions are modified in such confining environments remain open. Complex fluids confined to randomly interconnected porous networks are unique systems that permit addressing many challenging questions. For instance, extensive research at the confined superfluid transition that for many years was devoted to finite-size effect studies [1] has recently focused on the manner that quenched random disorder modifies the critical properties of the transition [2,3]. In fact, understanding why under silica aerogel confinement the critical exponents are modified by the disorder in a manner contrary to the expectations from the Harris criterion is of continuous experimental and theoretical interest. Equally interesting are results for a binary liquid mixture confined to a random porous media. The experimental evidence suggests that a ''random-field'' model could describe the modifications occurring at phase transitions [4–6].

Mostly during this decade, liquid crystals started to play a prominent role among physical systems being investigated under confinement. A number of researchers have used distinct liquid crystals and probed the effects that are introduced on them by different types of confining or host porous geometries. These confined liquid-crystal systems have been probed using a variety of experimental techniques [7–10]. The interest in this field is growing particularly because of the attractiveness that liquid crystals possess from both fundamental and applied points of view. The latter is of particular importance since, for example, constrained liquid crystals exhibit optical properties that can be suppressed by the application of an external field. It is well documented that the liquid-crystal optical properties have led to many useful applications. Fundamentally, they are relevant as confined liquid crystals are ubiquitous thermodynamic systems where a variety of different phase transitions under controlled quenched random disorder, or in well-defined geometries, can be studied. With liquid crystals, it is possible to accurately investigate configurational or phase transition, wetting and elastic properties, essentially, surface-induced phenomena under controlled conditions. The richness of these experimental systems has lately attracted considerable theoretical efforts [11–14].

Photon correlation spectroscopy experiments [7] with liquid crystals (LC) impregnating a random porous media showed that a random-field approach could equally be applied to interpret the dynamics of nematic ordering. Under those confining conditions, the nematic phase within the pores could be modeled as an Ising-like system (originally developed for magnetic spins) with an imposed random uniaxial field. The random uniaxial field is directly coupled to the orientational order parameter, *Q*, to account for the random confinement. Such a model uses a random uniaxial anisotropy on a spin system [11,12] including a symmetric coupling between the anisotropy vector and *Q* in order to account for the ''up-down'' symmetry of the nematic director. In general, these types of models may be described as random field Ising models or RFI.

Research efforts have also carefully evaluated how confinement affects thermodynamic properties. High-resolution calorimetric studies [9,10] have shown that the first-order phase transition that occurs in a parent bulk liquid-crystal material (like the nematic-to-isotropic or *N-I* transition), under certain confinement conditions, can be replaced by a smooth evolution to a glassy state. Such a glassy state is

characterized by a correlation length that does not exceed the pore size. Results of theoretical models using mean-field theory and Monte Carlo simulations [11] are in qualitative accord with the experimental findings. The smectic-*A* to nematic phase transition, Sm*A*-*N*, which in bulk belongs to the 3D-*XY* universality class, is drastically altered under confinement. For severe confinement conditions, as offered by some silica aerogel density, the magnitude of the specific-heat peak at the Sm*A*-*N* transition is highly suppressed, broadened over a wide temperature range, and shifted to lower temperature as the confining size is increased [8–10]. X-ray scattering studies have found scattering peaks at a q vector similar to that of the Sm*A* phase, indicating the presence of a structure with similar periodicity but considerably broader. This is consistent with severely restricted domains. The Sm*A*-*N* transition eventually disappears in nanometer-sized confinement. Alternatively, if the liquid crystal is subjected to less restrictive confining conditions, the second-order Sm*A*-*N* phase transition retains its sharp nature. It could nevertheless be affected by the confining host as in the case of the specific-heat critical exponent α that becomes size-dependent [9,10].

Recent studies suggest that RFI models may be applicable only when the ordered domains are much larger than the mean distance between disordering sites; macroscopic order is still possible for confinement sizes such that large interpore interactions dominate [13,14]. Experimental observations for binary liquid mixture systems that can be interpreted by a RFI model may also be described by phase wetting where the confinement is such that it inhibits the growth of an ordered phase domain [15]. However, an obvious difficulty of these static models is that they do not account for the extremely slow dynamics (long relaxation times) which are observed for order-parameter fluctuations. RFI types of models are further improved by implementing local correlations into them. Confining geometries where the pore structure minimizes the pore-to-pore interactions cannot be expected to follow the RFI model predictions [16–18]. For such cases, an appropriate approach is that of a single-pore (SP) model that considers ordering within single, independent pores. This is then averaged over the entire sample using a suitable distribution that describes the confining host [16,19].

The current investigation is devoted to a systematic study of the orientational order of octylcyanobiphenyl (8CB) liquid crystal confined to a series of silica aerogel samples. The density of the aerogel was varied from 0.068 to 0.6 g/cm^3 and the confined 8CB orientational order was probed with deuteron nuclear magnetic resonance (DNMR) spectroscopy. Each sample was studied as a function of temperature spanning the smectic-*A* (Sm*A*), the nematic (*N*), and isotropic (*I*) phases of 8CB. In this investigation we explored (i) the possibility of surface-induced orientational order in the isotropic phase; (ii) its behavior when the nematic phase is approached from high temperatures; (iii) how the *N*-*I* transition is altered by the random host media; and (iv) the type of nematic director structure, $\hat{n}(\vec{r})$, that can be sustained under confinement. How the orientational order and liquid-crystal structure were affected as the samples cooled into the Sm*A* phase was also carefully explored.

To highlight a few of the results fully described below, for all aerogel densities there is weak, remnant surface-induced orientational order in the isotropic phase which suggests a quasicomplete wetting of the silica strands and a homeotropic surface alignment. In the nematic phase, the DNMR spectral patterns are Pake powder patterns indicating that there are nematic domains of constant Q and randomized $\hat{n}$ by the isotropic structure of the aerogel host. The DNMR spectrum is dramatically different in the densest aerogel where only a single absorption peak is found whose width increases with decreasing temperature. This is interpreted as a continuous, gradual increase in average orientational order having a distribution of domains with different Q and $\hat{n}$, as first found under Vycor glass confinement. As the temperature is lowered, the enhancement in orientational order typical of the bulk Sm*A*-*N* transition is absent. This enhancement is in bulk related to the coupling between nematic and smectic order parameters, which is a function of the nematic range, 7 °C for 8CB. The lack of increase in Q at the Sm*A*-*N* transition suggests that the aerogel confinement induces a suppression of the Sm*A* phase and a weakening of the coupling between order parameters.

In this paper, we mostly focus on how the quenched disorder that is introduced by the host silica aerogel affects the liquid-crystal *N*-*I* transition; it is organized as follows. A brief overview on the experimental technique employed and how the confined samples are prepared is presented in Sec. II. In Sec. III, the experimental results for aerogel-confined 8CB in the isotropic, nematic, and smectic-*A* phases including DNMR spectral patterns, the scalar orientational order parameter, and its temperature dependence are presented. They are also discussed in light of other existing results. Conclusions and a summary of the results can be found in Sec. IV.

II. THE SOLID HOST, THE LIQUID CRYSTAL, AND THE TECHNIQUE

A. The solid host

The base-catalyzed silica aerogel consists of a random network of silica backbones in an openly connected void space. The aerogel samples used were prepared at MIT in Professor Carl Garland's laboratory following the exact same recipe to prepare all aerogel densities; we reproduce here the description of the aerogel host media that can also be found in [9]. Specifically, the silica aerogel was prepared from the base-catalyzed polymerization of tetramethylorthosilicate in methanol. This process yields a network structure with strut dimensions on the order of 10 nm and internetwork voids whose average dimension varies between 12 and 91 nm. The void sizes depend on the concentration of the precursor solution and on the degree of collapse during the drying. The wet gels are all dried supercritically except for the highest density (0.6 g/cm^3), which was partially air dried (or xerogelled) prior to the final supercritical extraction.

Small-angle x-ray-scattering studies (SAXS) have shown that these aerogels are fractal over a limited range of length scales [20]. For low-density aerogel, the scattering profile (or Porod behavior) reveals a fractal dimension of 2.0 ± 0.2. SAXS also showed that the silica backbones are smooth over length scales ranging between 1 and 5 nm.

TABLE I. Physical characteristics of the aerogel structure. Symbols: density ρ = the standard SiO_2 density, reduced density ρ_S = grams of SiO_2 per cubic centimeter of liquid crystal, mean void length L, porosity $\phi = L/d$, and the fraction of 8CB in direct contact with the SiO_2 surface $p = 2(l_b/L)$ [9,21]. ϕ and L are extrapolated SAXS values from [9] and $l_b = 2$ nm is the length of an 8CB molecule [24].

ρ (g cm^{-3})	ρ_S (g cm^{-3})	L (nm)	ϕ	p
0.068	0.073	91	0.95	0.04
0.115	0.128	57	0.93	0.07
0.124	0.138	53	0.92	0.08
0.172	0.197	43	0.90	0.09
0.265	0.318	26	0.85	0.15
0.330	0.408	21	0.82	0.19
0.493	0.605	14	0.76	0.29
0.600	0.822	12	0.73	0.33

The parameters that characterize each aerogel sample are summarized in Table I. The silica backbones are described in terms of an average solid chord d_S and a solid density ρ. The void space is given in terms of an average void chord, $L = \langle d_0 \rangle$, which represents the mean free path in the empty regions of the aerogel. The void (open) volume fraction or porosity ϕ given by $\phi = L/d$, with $d = L + d_S$ being the sum chord, specifies the fraction of the aerogel that can be filled with the liquid crystal [9,21]. Finally, it would be of interest to know the details of the void size distribution. However, this is difficult to obtain without destroying the sample. Nevertheless, an attempt using mercury porosimetry showed that the fractal aerogel network possesses a broad and relatively smooth distribution of void sizes [22].

B. The liquid crystal

For this investigation, we used the octylcyanobiphenyl liquid-crystal 8CB deuterated [23] at the first (alpha) position along the alkyl chain from the biphenyl group. Bulk 8CB, of molar mass 291.44 g/mol and molecular length $l_b \sim 2$ nm [24], exhibits the following phase transitions: the weakly first-order *N-I* orientational ordering transition at approximately $T_{N\text{-}I} \cong 40.8\,^{\circ}$C, and the second-order Sm*A*-*N* (*a* 1D translational ordering transition) approximately 7 °C below $T_{N\text{-}I}$. Bulk 8CB crystallizes via a strongly first-order transition at approximately 20 °C; under confinement, the transition to the crystalline phase is often substantially shifted to much lower temperatures. For this work, we chose 8CB because it has been well characterized in both bulk and in aerogel-confined form. The system has been extensively studied through a variety of experimental techniques including calorimetry, light and x-ray scattering, and dielectric spectroscopy, among others [7–10,25].

The filled aerogel samples were prepared in vacuum by heating the LC and aerogel just above room temperature but below the LC isotropic phase. This decreases the LC viscosity while filling and degassing both materials. The aerogel, in contact with the liquid crystal, was thus filled by capillary action. This slow ($\sim$ days long) process fully fills the voids (as determined by comparing the amount of 8CB absorbed to the available open volume) while preserving to the best extent possible the aerogel structure intact [9]. Once the aerogel filling process was completed, the outer surfaces of the aerogel samples were lightly dried with filter paper to minimize excess liquid-crystal bulk material. Finally, the samples were inserted (packed) and epoxy-sealed within a glass tube, 3 mm in diameter and 2.5 cm long.

C. The experimental technique

Nuclear magnetic resonance (NMR) is an extremely powerful tool for liquid-crystal research as it directly probes the orientational order Q, director configurations $\hat{n}(\vec{r})$, and molecular dynamics. Deuteron NMR, or DNMR, has been extensively and successfully applied to bulk studies [26] and also to liquid crystals confined to well-defined cylindrical pores, or to random interconnected porous geometries [22,27–29].

The DNMR spectrometer employed in this study consists of a 4.7 T (200 MHz for protons, 30.8 MHz for deuterons) superconducting magnet fitted with a homemade probe tuned to deuterium, and commercially available electronics. The probe head is inserted in an oven housed in the magnet bore, through which a mixture of ethylene glycol and water circulates from an external temperature controlled bath. The probe head is provided with a calibrated 100 Ω platinum thermometer that is read after each DNMR pulse sequence and averaged over the thousands of scans accumulated in the process. The temperature stability over the entire DNMR spectra acquisition time is better than 0.050 °C with a resolution of $\pm 0.005\,^{\circ}$C.

All 8CB aerogel-confined samples were subjected to the same thermal history within the DNMR probe. After thermally cycling the sample several times through the *N-I* transition in the presence of the DNMR field and keeping the sample overnight at a temperature above $T_{N\text{-}I}$, measurements were performed first cooling then heating. Some arbitrarily chosen 8CB-aerogel samples were studied again months apart, to ensure reproducibility.

DNMR measurements used a quadrupole-echo pulse sequence [$(90°)_x$-τ-$(90°)_y$-τ-acquisition] with full phase cycling: $\tau \cong 100\,\mu$s, $90° \cong 3\,\mu$s, a 1024–2048 point acquisition, and a last delay of 300 ms (which prevents T_1 saturation). This sequence was accumulated for as many as 50 000 scans over a 4.5-h period. The final spectrum is obtained by a complex Fourier transform of the single zero-filled free induction decay (FID) with no line broadening.

D. DNMR spectra of liquid crystals

It is well known that the NMR spectrum from a domain of molecules with uniform director, in particular a nematic liquid-crystal compound deuterated at a specific site, consists of two sharp absorption lines separated in frequency by [26,30]

$$\delta\nu = \tfrac{1}{2}\,\delta\nu_0 Q(3\cos^2\theta_B - 1). \tag{1}$$

Here $\delta\nu_0$ is the maximum frequency splitting observable in a fully aligned bulk nematic sample, Q is the scalar order parameter, and θ_B is the angle that the nematic director $\hat{n}$ makes with the static magnetic field $\vec{B}_0$. For bulk, $\theta_B = 0°$ due to the magnetic-field-induced uniform alignment of $\hat{n}$.

For sufficiently confined liquid crystals, the splitting has a positional dependence, $\delta\nu=\delta\nu(\vec{r})$, through a director structure $\theta_B=\theta_B(\vec{r})$ as well as through a scalar order-parameter structure $Q(\vec{r})$. Equation (1) is then recast in the form

$$\delta\nu(\vec{r})=\tfrac{1}{2}\delta\nu_0 Q(\vec{r})[3\cos^2\theta_B(\vec{r})-1]. \tag{2}$$

To illustrate, when all molecules are aligned parallel to the external magnetic field, $\theta_B=0°$ and from Eq. (2) we find that $\delta\nu=\delta\nu_B=\delta\nu_0 Q$. Alternatively, with all molecules perpendicular to the field, $\delta\nu=\frac{1}{2}\delta\nu_B=\frac{1}{2}\delta\nu_0 Q$ given that $\theta_B=90°$. It should be emphasized that the director structure dictated by the porous aerogel host is unaffected by the external magnetic field if the confining length L (the aerogel void size) is smaller than the magnetic coherence length ξ_M. The magnetic coherence length can be calculated from [26,27]

$$\xi_M=\left(\frac{\mu_0 K}{B_0^2\Delta\chi}\right)^{1/2}\approx 1\ \mu\text{m}. \tag{3}$$

In Eq. (3), K is the average Frank elastic constant (single elastic constant approximation) and $\Delta\chi$ a measure of the anisotropy of the magnetic susceptibility. From Table I, for all aerogel samples, ξ_M is much larger than L and the director structure is solely determined by the host.

Reiterating, for a typical bulk-nematic liquid-crystal sample, the DNMR spectral pattern consists of two sharp absorption lines, typically 10–100 Hz of full width at half maximum (FWHM), separated in frequency by an amount $\delta\nu_{\text{bulk}}=\delta\nu_0 Q$, the quadrupolar splitting. For a confined sample with a single scalar order-parameter Q which is often smaller than bulk's, but with an isotropic angular distribution in $\hat{n}$, a Pake powder pattern is found. For an isotropic angular distribution of $\hat{n}$ with a constant Q, shoulders appear at a frequency splitting equivalent to $\delta\nu_{\text{bulk}}$, in addition to 90° (or $\pi/2$) singularities separated by a frequency splitting of $\frac{1}{2}\delta\nu_{\text{bulk}}$ [26,30]. If a distribution in Q not centered at $\overline{Q}=0$ also exists, what would be observed is a superposition of powder patterns with different singularity splittings $\delta\nu_{1/2}=\frac{1}{2}\delta\nu(Q)$. This results in the smearing of the two singularities into two inhomogeneously broadened absorption peaks; the broad peaks have a frequency separation $\frac{1}{2}\delta\nu_0\overline{Q}$. If the distribution in Q is narrow and centered at $\overline{Q}=0$, then a single and sharp inhomogeneously broadened peak would be obtained. Such a single peak would be quantified by a FWHM approximately equal to 50 Hz. A single and narrow absorption peak in fact represents the usual NMR spectral pattern for an isotropic liquid crystal.

The previous description does not take into account the possibility of the existence of defects, small regions of approximately 10 nm in diameter where $Q\approx 0$, nor the effects of motional diffusional averaging. In fact, it is well established that DNMR spectra are sensitive to the type of orientational ordering (as seen above) and to motional narrowing. As discussed by Zidansek *et al.* [22], in aerogel, motional narrowing is mostly due to the translationally induced rotation of liquid-crystal molecules [31]. Whether motional averaging is significant to the extent of influencing the NMR pattern depends on the length scale L (for instance, comparable to the mean void length) over which $\hat{n}(\vec{r})$ and $Q(\vec{r})$ exhibit substantial variation. This length scale is to be compared against x_0, which is estimated from $x_0\approx(D/Q_B\delta\nu_0)^{1/2}$. Here x_0 effectively measures the average distance that a molecule migrates over the time scale of the NMR measurement. In the above expression, D is the average translational diffusion constant. The DNMR spectra are thus fully time-averaged but they are only spatial-averaged over a distance x_0.

Depending on the type of confining conditions, translational diffusion might be inhibited, particularly for a thin liquid-crystal layer in contact with a solid substrate. However, for local averaging over a single void, the diffusion constant can be taken to be that of the bulk liquid crystal, or specifically for nematic 8CB, $D\cong 10^{-11}\,\text{m}^2/\text{s}$, and $Q_B\delta\nu_0\cong 40\,\text{kHz}$. We then find that in the nematic phase, $x_0\approx 15\,\text{nm}$; in the isotropic phase, x_0 is an order of magnitude larger or ≈150 nm [27–31]. Thus, if $Q(\vec{r})$ is approximately constant over the confining void size, the DNMR spectra reflect the real static director structure. If $Q(\vec{r})$ varies substantially, as in the case of defects spaced closer than x_0, the DNMR spectra will include considerable motional narrowing of all features, directly reflecting the decrease in orientational order. In short, director field distortions are expected to extend over a length scale determined by the confining size, here the aerogel mean void length L. Motional averaging is more likely negligible in samples for which $x_0 \ll L$ is satisfied. As seen in Table I, the 8CB-aerogel system fails to satisfy this condition, so some motional narrowing is expected, particularly in the densest aerogels.

III. RESULTS AND DISCUSSION

Whether confinement substantially affects the liquid-crystal physical behavior or the type of structural configuration displayed by the liquid-crystal molecules within the host strongly depends on the morphology and typical length scales of the host media, and on the anchoring energy and elastic distortions characterizing the host surface interactions with the liquid crystal. Phase transitions are affected differently according to the order of the parent bulk transition and/or the nematic range; the order of the transition or the specific-heat critical exponent can be altered by the confinement. A relevant parameter that we have identified and that helps to quantify the confinement effects is the nematic correlation length ξ_N. At $T_{N\text{-}I}$, the nondiverging ξ_N for 8CB grows to approximately 15 nm [32], which is of the same order as the diffusion length x_0 in the aerogel host.

In this study, we determined the NMR spectral patterns for 8CB confined to aerogel samples, eight of them, of different silica density. The confining size or mean void length L is decreased from 91 nm, which is six times larger than ξ_N, to 12 nm, which is slightly less than ξ_N. Another length scale is the micron-sized magnetic coherence length, which, as stated earlier, is much larger than the confining sizes used and thus is not particularly relevant in these measurements. Therefore, the director structure is determined by the solid host; however, motional averaging does play a role. For all 8CB+aerogel samples, the spectra are temperature dependent and independent of sample orientation with respect to

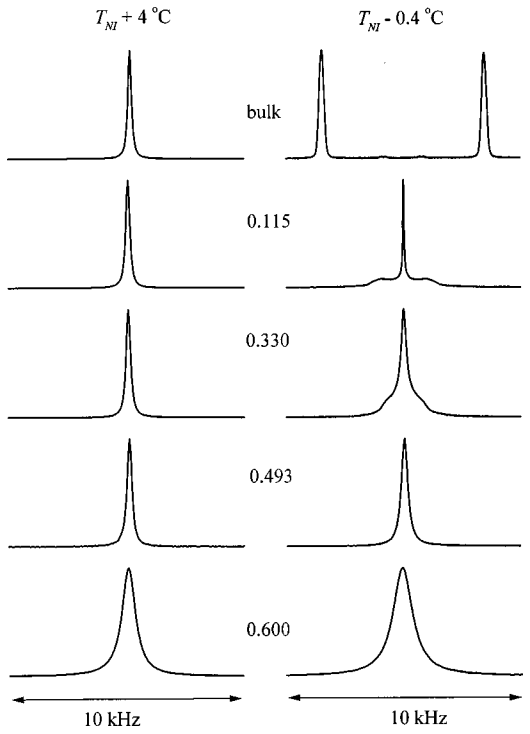

FIG. 1. DNMR spectral patterns for bulk and some of the aerogel-confined samples at two temperature bracketing $T_{N\text{-}I}$. A few degrees above $T_{N\text{-}I}$, the increase in width of the line with increasing density, most obvious for the densest aerogel, reflects a remnant surface-induced ordering. The frequency scale for the upper three right spectra has been divided by a factor of 6. The numbers in the middle represent the aerogel density in g/cm^3.

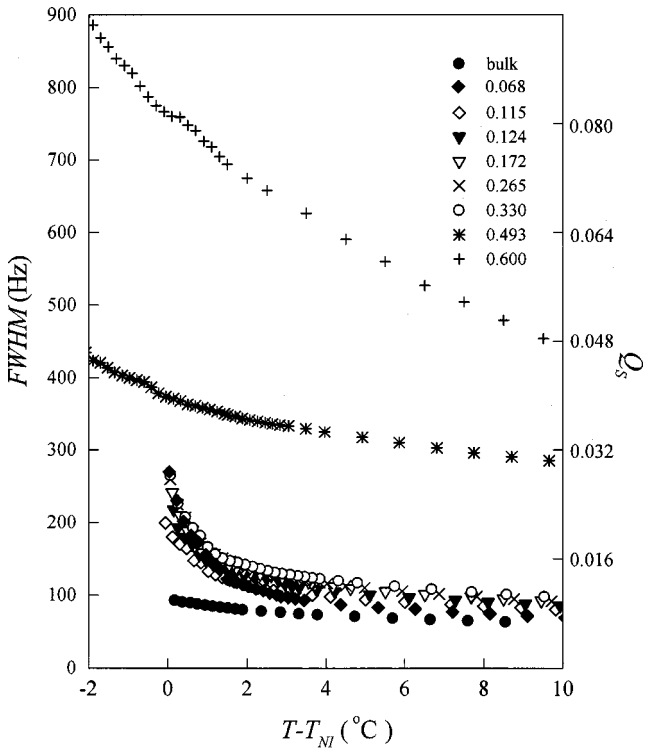

FIG. 2. Dependence on temperature and silica density of the FWHM of the isotropic single absorption peak for bulk and confined samples. The degree of surface ordering is also evaluated and is provided on the right axis. For clarity, the 0.493 g/cm^3 data have been shifted up by 100 Hz. For $T \geq T_{N\text{-}I} + 3$ °C, the FWHM monotonically increases with increasing density. This is also the case closer to $T_{N\text{-}I}$ if the 0.068 sample is excluded. In addition, near $T_{N\text{-}I}$ there is a temperature dependence that is stronger than the bulk's and may be interpreted as a manifestation of quasicomplete orientational-order wetting.

the NMR field; the latter is expected given the isotropic nature of the host aerogel structure.

A. Isotropic phase

The DNMR spectra at temperatures corresponding to the bulk isotropic phase are a single absorption peak for all aerogel densities studied; only a few characteristic examples of these peaks are presented in Fig. 1. The confined peak is broader than the corresponding bulk isotropic peak; for instance, for the 0.6 g/cm^3 aerogel it is three to four times broader at temperatures well above $T_{N\text{-}I}$. The FWHM of the isotropic peak is dependent on silica aerogel density; it is also dependent on temperature; in cooling towards the nematic phase, it becomes more strongly temperature dependent. The density and temperature dependence of the FWHM for $T > T_{N\text{-}I}$ for all aerogel-confined samples studied is presented in Fig. 2.

The presence of a single absorption DNMR isotropic peak that is broader than bulk's is typically found for confined liquid crystals. Through DNMR, such a phenomenon was originally observed in the cylindrical and parallel pores of Nuclepore and Anopore membranes [27,30,33]; the same effect was later found in aerogel [16,22,28], Vycor-like glass [34], and Millipore [10,29]. It is not related to the degree of randomness of the host porous media. This remnant, nematiclike order in the isotropic phase is sometimes referred to as paranematic order. It arises from the interaction between the liquid crystal and the imbedded solid surface that induce a finite Q_S within a surface layer of thickness comparable to the liquid-crystal molecular length. This effect depends on the strength of the anchoring energy. However, since such surface interactions are local in nature, they typically yield a weak temperature dependence of Q_S in the isotropic phase.

The degree of ordering Q_S induced by the surfaces can be correlated with the line-broadening FWHM and applied to the results shown in Fig. 2. The linewidth $\mathcal{F}_{\mathrm{ISO}}$ in the isotropic phase broadened by surface-induced ordering can be approximately obtained from [35]

$$\mathcal{F}_{\mathrm{ISO}} \approx l Q_S \Delta\nu_0 \left(\frac{\pi Q_S \Delta\nu_0}{D} \right)^{1/2} . \tag{4}$$

In Eq. (4), l is the thickness of the surface layer, usually taken to be about 4 nm. Solving for Q_S from Eq. (4) it is found that a 150-Hz linewidth corresponds to approximately $Q_S = 0.016$. Evidently, there is surface-induced order that survives to temperatures well above $T_{N\text{-}I}$. As the temperature is lowered towards $T_{N\text{-}I}$, a nematic layer wets the aerogel surfaces long before the phase transition occurs. This agrees with the earlier conclusions from similar DNMR (obtained with a different magnetic-field strength) results obtained for two aerogel samples of larger mean void size that also included lecithin treatment of the surface [22].

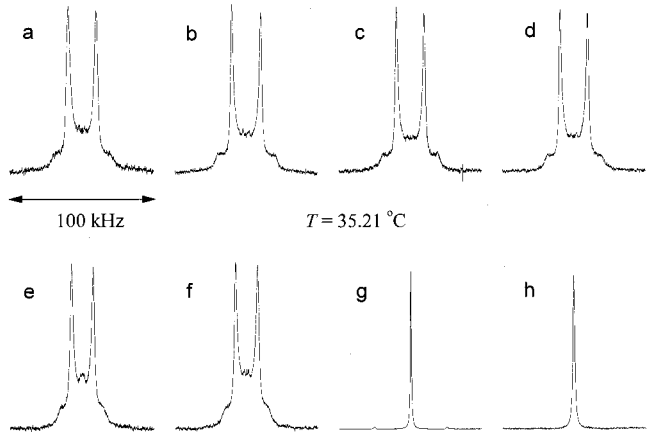

FIG. 3. DNMR spectra for 8CB+aerogel at a temperature corresponding to the bulk nematic phase, $T=35.21\,^{\circ}\mathrm{C}$. The densities are 0.068, 0.115, 0.124, 0.172, 0.265, 0.330, 0.493, and 0.600 g/cm^3 for a, b, c, d, e, f, g, and h, respectively.

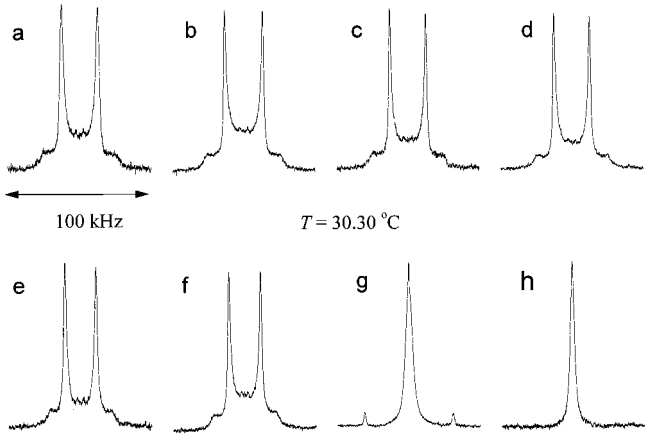

FIG. 4. DNMR spectra for 8CB+aerogel at a temperature corresponding to the bulk smectic phase, $T=30.3\,^{\circ}\mathrm{C}$. The small splitting seen in g is due to bulk material residing on the outer surfaces of the sample. Legend as in Fig. 3.

Figure 2 reveals additional interesting features. The FWHM for all samples lies above bulk's and, except for the two denser aerogels, almost collapses on top of one another. For $\rho \leqslant 0.33$ g/cm^3 and $T-T_{N\text{-}I}>3\,^{\circ}\mathrm{C}$, the temperature dependence of the FWHM of the confined samples is weak and in fact it effectively mimics bulk's. In this temperature regime and at constant temperature it increases with silica density. As $T_{N\text{-}I}$ is approached (excluding the 0.068 sample) the increase in width with density is retained. There is also a considerable deviation from the bulk behavior and much stronger temperature dependence: the confined FWHM increases rapidly with decreasing temperature in a manner that is suggestive of quasicomplete orientational-order wetting of the aerogel surfaces. This should be contrasted with the situation where partial wetting occurs; there, as the temperature decreases, the FWHM of the isotropic peak exhibits a weak temperature dependence similar to bulk's. Alternatively, for complete wetting conditions, the FWHM would diverge at $T_{N\text{-}I}$ [36]. Then, a quasicomplete orientational-order wetting situation appears to better describe the behavior in aerogel.

A systematic study of the orientational-order wetting of a solid interface was performed in Anopore membranes treated with several aliphatic acids of variable chain length; these yielded different liquid-crystal anchoring conditions [36]. Such study revealed that partial wetting occurred mostly under parallel anchoring conditions while quasicomplete wetting was found for homeotropic anchoring conditions. Thus, by comparison to our current results, the 8CB molecules are primarily aligned perpendicularly to the aerogel strands. Homeotropic anchoring conditions are expected for a cyanobiphenyl liquid crystal like 8CB at a SiO_2 surface due to the presence of —OH surface groups and the polar nature of the liquid crystal [37]. Nevertheless, the same DNMR patterns would be obtained regardless of the local molecular orientation at the silica strands. The isotropic structural nature of the aerogel host would randomize the director $\hat{n}$ in both cases.

The FWHM for the two denser aerogels, and particularly that for the 0.6 g/cm^3 density, in addition to being broader and thus reflecting that Q_S increases with increasing density, also exhibits a stronger temperature dependence near the *N-I* transition. At all temperatures, 8CB in these aerogel densities behave in a considerably different manner than in the lesser dense gels as discussed below. Both high densities show an apparent ''kink'' in the FWHM temperature dependence at a temperature near the bulk $T_{N\text{-}I}$, but neither shows a true transition to the nematic phase. Their behavior consists of a continuous evolution of orientational order [17,18].

B. Nematic and smectic-*A* phases

Decreasing the temperature and crossing into the nematic phase, and eventually the smectic, produces the DNMR spectral patterns that are shown in Figs. 3–6. In those figures, we present the intensities of the spectra at four different temperatures. Specifically, we show DNMR spectra at 35.21 °C corresponding to the bulk nematic phase, 30.30 and 25.25 °C both corresponding to the bulk smectic-*A* phase, and 20.56 °C near bulk freezing. It is quite conclusive from the patterns that a nematic phase is formed in the aerogel host. It is characterized by a single Q and an isotropic distribution of $\hat{n}$.

The DNMR spectra for all aerogel samples of density $\rho < 0.493$ g/cm^3 are well-resolved Pake powder patterns with

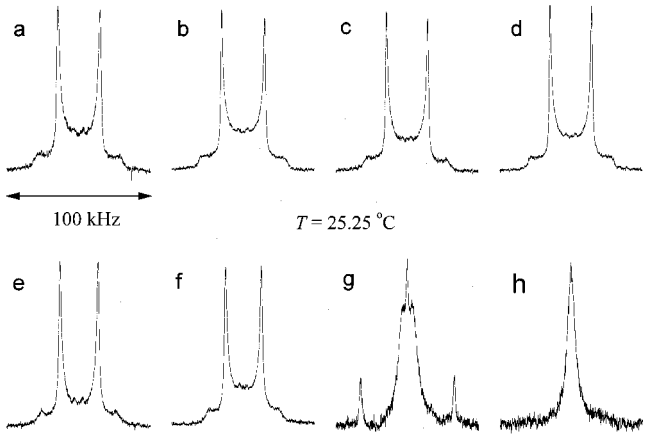

FIG. 5. DNMR spectral patterns for 8CB+aerogel at a temperature also corresponding to the bulk smectic phase, $T=25.25\,^{\circ}\mathrm{C}$. Notice the splitting in the central peak for the 0.493 sample. Legend as in Fig. 3.

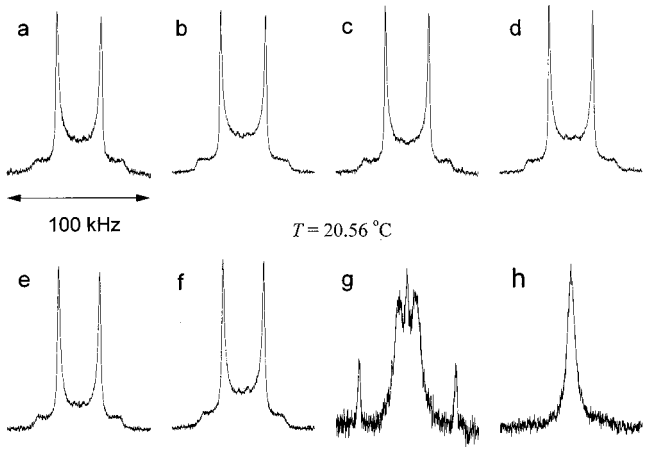

FIG. 6. DNMR spectra for 8CB+aerogel at $T=20.56\,^{\circ}\mathrm{C}$, a temperature at which bulk 8CB has solidified while 8CB+aerogel is supercooled considerably [8]. Legend is as in Fig. 3.

two low-intensity shoulders separated in frequency twice as much as the two high-intensity $\pi/2$ singularities. The frequency separation between the $\pi/2$ singularities (or equivalently that between the shoulders) is temperature dependent. The spectra powder pattern is retained for all samples down to the lowest temperature shown of $T=20.56\,^{\circ}\mathrm{C}$. Over the temperature range of our DNMR studies we found no evidence of liquid-crystal freezing. This is expected since it is known from x-ray-scattering measurements that the freezing transition of 8CB in aerogel could be supercooled by as many as $20\,^{\circ}\mathrm{C}$ [8].

As expected, the DNMR spectra observed are independent of sample orientation with respect to the static NMR field. This, and the Pake powder patterns, indicates that the nematic phase contains domains with an isotropic distribution of the director $\hat{n}(\vec{r})$ and a single spatially homogeneous value of Q. Given the aerogel isotropic structure, it should be expected that all orientations of $\hat{n}(\vec{r})$ occur with equal probability. Also, this suggests that the aerogel void size distribution does not play a significant role, only that the voids are highly interconnected. The average size of the nematic domains cannot be determined from these line shapes; any combination of domains with an isotropically distributed director $\hat{n}(\vec{r})$ would yield similar powder patterns. The Pake patterns do imply that the nematic domains are large compared to the diffusion length so that few molecules diffuse from one domain to another during the FID. Recent quasielastic light-scattering results [38] showed that there are nematic correlations that take place over length scales approaching $\sim$100 average void sizes. This collective behavior extending over several confining sizes is also common to other confined systems. Order correlated to length scales greatly exceeding the confining size has been found at the helium superfluid transition in both Vycor and aerogel [2,3].

The DNMR patterns for the 0.493 and 0.6 g/cm^3 aerogel samples show a (seemingly) drastically distinct behavior when compared to the less dense aerogel samples. At temperatures corresponding to the nematic and smectic-A phases, $T=35.21\,^{\circ}\mathrm{C}$ (Fig. 3) and $30.23\,^{\circ}\mathrm{C}$ (Fig. 4), respectively, the spectra are isotropiclike, similar to those in Fig. 1. The line shapes reveal a single, central, absorption peak whose FWHM continuously increases with decreasing temperature. If the temperature is further decreased to $T=25.25\,^{\circ}\mathrm{C}$ (see Fig. 5), while the FWHM for the 0.6 sample monotonically increases, for the 0.493 aerogel sample, a small splitting superimposed on a broad central peak appears. The splitting grows upon cooling, as seen at $T=20.56\,^{\circ}\mathrm{C}$ shown in Fig. 6. Also, for the 0.493 aerogel, a pair of very small peaks that first appeared in Fig. 3 have now clearly emerged as nematiclike quadrupole splitting peaks, widely separated in frequency. The intensity and frequency separation of this small splitting increases with temperature. This small splitting arises from remnant bulk material on the outer aerogel surface and is not related to any confinement effect.

The behavior in the 0.493 sample can be understood as follows. For this density, the mean void size is $L\approx 14\,\mathrm{nm}$, which is close to the translational diffusion length, $x_0\approx 15\,\mathrm{nm}$. Therefore, translational diffusion motion is now fast enough to cause considerable narrowing (translationally induced rotation mechanism [31]) in the resulting spectra. The absorption spectra would be affected if [39]

$$\varepsilon \cong \frac{\Delta\nu L^2}{6D} \leqslant 10. \tag{5}$$

Using typical values, we find for this sample that $\epsilon \leqslant 1$. Consequently, the DNMR spectrum is strongly affected by motional narrowing [40] that produces the single broad peak. Lowering the temperature slows the molecular diffusion such that a splitting is eventually resolved. The pronounced sharp central peak, clearly seen in Figs. 5 and 6, can be attributed to defects, regions of $Q\approx 0$ order. At a defect site, the director field changes considerably, and due to the local spatial averaging, the DNMR spectrum would reveal a central peak [16].

An alternative scenario must be considered. Suppose now that $Q\neq 0$ and that motional diffusion is significant. For the weak diffusion case $x_0 \gg \sqrt{D/Q_B\delta\nu_0}$, one would observe powder-pattern singularities. In the limiting case of strong diffusion, or $x_0 \ll \sqrt{D/Q_B\delta\nu_0}$, only a sharp central line would be observed. However, should motional diffusion be intermediate between those limiting cases, equivalently $x_0 \approx \sqrt{D/Q_B\delta\nu_0}$, the superposition of both the central peak (strong diffusion) and the two singularities (weak diffusion) would yield the DNMR pattern. To distinguish which explanation better adheres to the experimental results, measurements of the ''Hahn spin-echo'' T_2 [41], which are not currently available in aerogel, would be required.

The DNMR spectra for the 0.6 g/cm^3 aerogel, with average mean void length $L=12\,\mathrm{nm}$, is a single absorption peak at all temperatures. The FWHM of this peak, 450 Hz (three to four times broader than bulk's) at a temperature $10\,^{\circ}\mathrm{C}$ above its $T_{N\text{-}I}$, monotonically increases to approximately 10 kHz at $20\,^{\circ}\mathrm{C}$ below $T_{N\text{-}I}$. This behavior is reminiscent of that found for cyanobiphenyls confined to the 7 nm Vycor glass pores [17]. In particular, for 5CB in Vycor, a single peak of width increasing from 700 Hz at temperatures well above $T_{N\text{-}I}$ to 5.8 kHz at $T_{N\text{-}I}-T=14\,^{\circ}\mathrm{C}$ was found. Effectively, the N-I phase transition is replaced by a continuous evolution of orientational order in the pores. Such a glassylike orientational order as evidenced by the broad absorption spectra is for the most part locally determined.

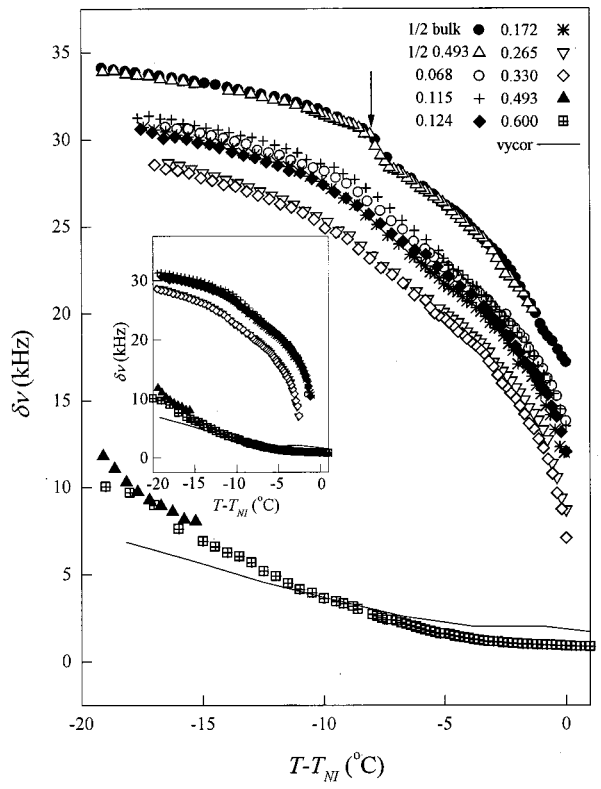

FIG. 7. Temperature dependence of the frequency separation between the $\pi/2$ singularities of the powder patterns. Also plotted are $\frac{1}{2}$ of the bulk nematic splitting and the FWHM of the single peak of the 0.6 aerogel. For the 0.493 aerogel, what is plotted is (a) the inner splitting (first seen 15 °C below $T_{N\text{-}I}$, Fig. 5) and (b) the outer splitting. The scaled 5CB in Vycor results [17] are also included. Inset: same data except that for some of the aerogels the temperature scale has been shifted. Note the nearly perfect overlap effectively separating the confined behavior into three density regions.

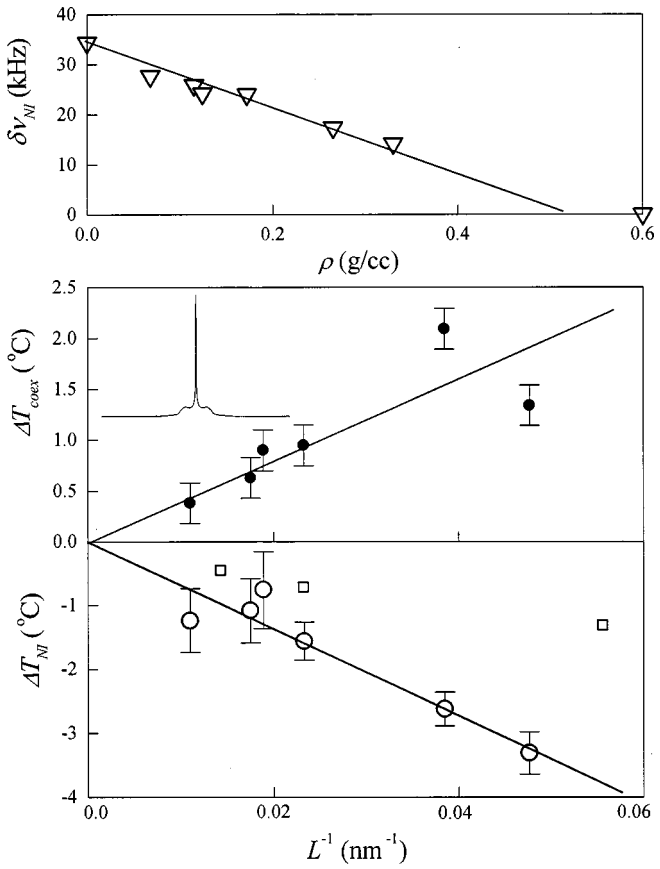

FIG. 8. The discontinuous jump in frequency splitting at $T_{N\text{-}I}$ as a function of silica density (top); the $N+I$ coexistence width (middle) including a typical DNMR pattern, and (bottom) the transition temperature shift from bulk as a function of inverse confining size L^{-1}. The solid lines are guides to the eye. In the bottom panel, the open squares are the specific-heat results from [9].

The temperature dependence of the $\pi/2$ splitting and FWHM is illustrated in Fig. 7 for all 8CB+aerogel samples studied. For aerogel samples in the density range between 0.068 and 0.33 g/cm^3, what is plotted is the $\pi/2$ splitting. For the 0.493 aerogel, both the FWHM and the $\pi/2$ splitting are plotted. For the 0.6 aerogel density what is shown is the continuously increasing FWHM of the single peak. The 5CB Vycor results [multiplied by $\delta\nu_{\text{bulk}}(8\text{CB})/\delta\nu_{\text{bulk}}(5\text{CB})=1.17$] and $\frac{1}{2}$ of a fully field aligned bulk 8CB are also included for comparison.

From Fig. 7 it can be seen that the 0.6 aerogel and Vycor (and also the 10-nm microporous fused or Vycor-like glass studied in [34]) behave similarly. This confirms the continuous growth of orientational order that we alluded to earlier. What is common to both porous hosts is that their mean void size is less than the nematic correlation length. As further discussed below concerning Fig. 9, we find that how the confining length compares with ξ_N determines what type of behavior will be found in the confined system.

For silica densities less than 0.6 and at low temperatures, the frequency splitting is suppressed by 15–20 % as compared to bulk; overall, the trend is that of greater suppression with increasing aerogel density; the frequency splitting decreases to $\sim\frac{1}{3}$ of the bulk value for the 0.493 density. The aerogel surfaces tend to suppress the nematic order in the nematic phase. The enhancement of orientational order as the temperature is decreased into the smectic-A phase does not occur in these confined samples. We take this to suggest that the aerogel confinement (as Millipore [10] and aerosil [9] also do) weakens the coupling between nematic and smectic order parameters since, as determined from x-ray studies [8], some form of smectic phase does remain without the saturation of Q. The lack of a sudden increase in orientational order is also consistent with the broadening and eventual disappearance of the SmA-N phase transition [9]. It is difficult to visualize how a well-defined layered structure can be formed under such tortuous and restrictive confining conditions. Elastic distortions, increasing with decreasing size, could conceivably prevent a smectic from forming.

Noticeable from Fig. 7 at the N-I transition, one observes the typically discontinuous jump from an isotropiclike single peak to a quadrupolelike nematic splitting. The size of the jump decreases with increasing aerogel density, and is nonexistent for the highest density samples. This is further illustrated in the top panel of Fig. 8, where we plot the size of the frequency-splitting jump at the N-I transition temperature as a function of silica density. To within experimental accuracy, the size of the jump, $\delta\nu_{N\text{-}I}$, decreases linearly with silica density. It extrapolates to zero at a ''critical'' silica density of approximately 0.5 g/cm^3 and $L\approx x_0\approx\xi_N$. Therefore, with increasing density or decreasing confining size, the weakly

first-order *N-I* phase transition becomes gradually less discontinuous and is eventually replaced by a smooth evolution of orientational order.

It can be shown that the aerogel-confined samples exhibit a similar behavior depending on the silica density range. This is visualized in the inset of Fig. 7, where we show the same frequency splitting except that for some densities it has been translated only in temperature. Given the excellent overlap of the sets of data, particularly for temperatures corresponding to the nematic phase, the results can be grouped as (a) $0.068 \leqslant \rho \leqslant 0.172$; (b) $0.265 \leqslant \rho \leqslant 0.330$; and (c) $\rho \geqslant 0.493$. The highest density region could also include Vycor. Grouping the data in this way may allow quantifying the amount of quenched disorder introduced by the aerogel. With increasing silica density (equivalently, increasing quenched randomness), the nematic order is at first somewhat suppressed [region (a)], then it is further suppressed [region (b)], and finally it is so largely suppressed that there are no phase transitions but only a gradual evolution of order [region (c)].

These density regions of different behavior can also be connected to the relevant length scales for the confined system. For densities corresponding to region (a), the void size L is greater than three times the thermal nematic correlation length; in density region (b), L is slightly larger than ξ_N; finally, in region (c), L is less than ξ_N. This effect is illustrated in Fig. 9, where Q is plotted as a function of inverse pore size; in such a plot, bulk corresponds to the y intercept and the three different regions stressed with horizontal solid lines. After a decrease in Q with L^{-1}, a considerable jump representing a drastic decrease in orientational order occurs for mean void sizes comparable to ξ_N. In short, these empirical results suggest that how substantially the bulk behavior is affected by the porous media depends on how the mean confining size compares with the nematic correlation length.

Another aspect of this aerogel systematic study that we wish to address is the $T_{N\text{-}I}$ dependence on silica density. In general, for confined liquid-crystal systems, transition temperature shifts can be due to elastic distortions, surface (anchoring) interactions, and finite-size effects. Theoretically, elastic distortions always shift $T_{N\text{-}I}$ down with an L^{-2} dependence while surface interactions either decrease or increase the transition temperature depending on the surface ordering properties and topology. Finite-size effects are expected to decrease the transition temperature, but for these systems, since the nematic order exceeds L, finite-size effects should not play a significant role. Specifically for the 8CB+aerogel system, specific-heat results have shown that $T_{N\text{-}I}$ decreases linearly with the inverse confining size L^{-1} [9]. Although DNMR is not the ideal probe to accurately determine transition temperatures, in the bottom panel of Fig. 9 we plot the difference between the bulk and the confined $T_{N\text{-}I}$ transition temperatures. To within the large error bars in the DNMR measurement, the shift in transition temperature dependence L^{-1} is linear. The slope is a factor of ~ 2 different from that obtained in the specific-heat study [9]; this may be attributed (see also below) to the different aerogels used in the two experiments. Nonetheless, what we believe is significant is the $T_{N\text{-}I}$ linear dependence on inverse confining length.

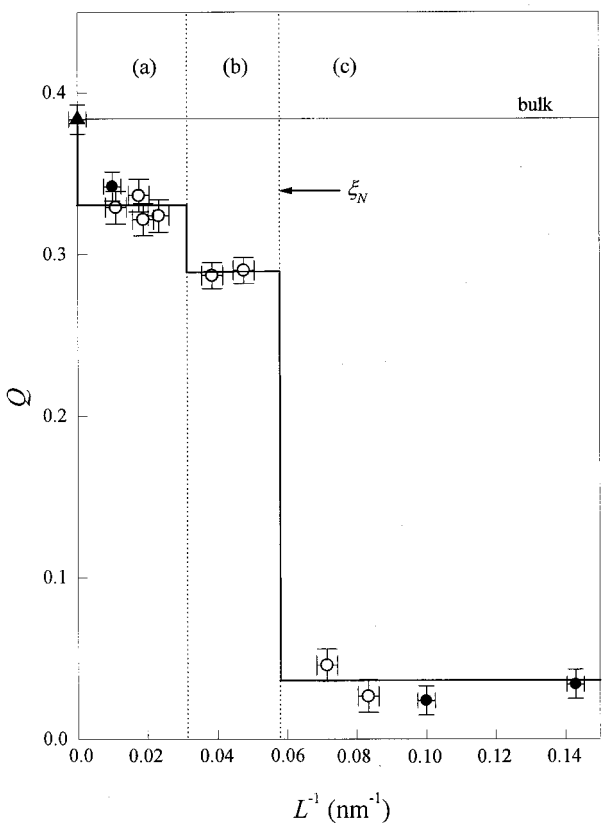

FIG. 9. The dimensionless nematic scalar order parameter calculated at $T = 28\,^{\circ}\mathrm{C} \ll T_{N\text{-}I}$ as a function of inverse confining size L. Note the sharp decrease when the confining size is comparable to the nematic correlation length. The open symbols are these aerogel results; the solid circles represent Vycor glass [17] and the Vycor-like fused glasses [34] while the triangle represents bulk. Regions (a), (b), and (c) are the density regimes of similar behavior first noted in the inset to Fig. 7 (see also text). The thick solid lines are guides to the eye to stress the existence of these different aerogel density regions of similar confined behavior.

The difficulty in determining the confined $T_{N\text{-}I}$ from a DNMR measurement can be further illustrated. In the middle panel of Fig. 8, or the right column of Fig. 1, we see that the confined DNMR spectra near $T_{N\text{-}I}$ consist of a central peak and two shoulders. In bulk, the isotropic single absorption peak would be replaced by the quadrupole splitting. In aerogel, the pattern likely represents the coexistence of isotropic and nematic phases; however, specific-heat results indicate that the width of the coexistence region is about 0.3 °C for the lowest density aerogel. The pattern may also indicate effects from motional narrowing which turn the $\pi/2$ singularities into a single peak. However, the FWHM of this central peak would have to be one-half of the frequency separation between the shoulders, which is not the case here. The pattern may also indicate that there is a void size distribution where $T_{N\text{-}I} = \langle T_{N\text{-}I}(R) \rangle$ and R represents a particular void size. What may be of interest is that (see the middle panel of Fig. 8) the temperature width of the ''coexistence'' region depends linearly on L^{-1}. Since L^{-1} is proportional to the aerogel density [9], the width of the ''coexistence'' region is directly proportional to the silica density.

In recent specific-heat results [9], it is found that the con-

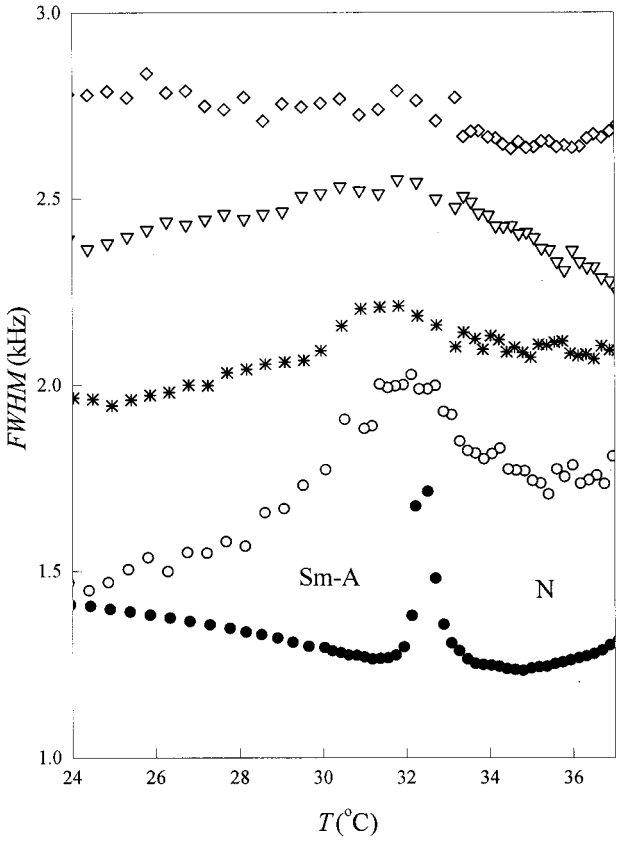

FIG. 10. Temperature dependence of the FWHM of one of the $\pi/2$ singularities of the powder spectra of the confined samples (or one of the absorption peaks for the bulk quadrupole splitting). Notice the change in width and shape at the SmA-N transition: the sharp peak seen for the bulk sample becoming broader and smaller with increasing density, disappearing for the highest density shown. This behavior is reminiscent of that of the specific heat [9]. In ascending order, the data are bulk, 0.068, 0.172, 0.265, and 0.33 g/cm^3. The data have been shifted slightly for clarity.

fined SmA-N phase transition becomes broad, is highly suppressed, and is eventually eliminated with increasing density. Although the enhancement of orientational order that occurs at $T_{\mathrm{Sm}AN}$ is not present, we have empirically found another way in which the DNMR results yield qualitative information on the existence or lack of SmA-N phase transition. For the aerogel densities that show powder spectra, it is possible to determine the FWHM of one of the absorption peaks (the $\pi/2$ singularities) as a function of temperature. This is shown in Fig. 10 for bulk and a few aerogel samples. The FWHM is related to the NMR time scale T_2, the spin-spin relaxation rate. From Fig. 10 (data shifted upwards for clarity) one sees that for bulk there is a well-defined sharp peak, which is found at a temperature that is consistent with T_{AN}. With increasing aerogel density, this peak becomes rounded, broader, and suppressed compared to bulk. For the densest aerogel shown, there is a featureless FWHM over the entire temperature range shown. If we associate the presence of the peak with the SmA-N phase transition, then no transition has occurred in the 0.6 aerogel sample. Overall, although the temperature width over which the FWHM changes is much narrower than that of the specific-heat peak, its dependence on aerogel density is reminiscent of that of the specific heat shown in Fig. 7 of Ref. [9].

A final issue can be addressed. From Fig. 10, the baseline value of the FWHM increases with density. Although the data have been shifted, if we exclude the lowest density aerogel (for some unknown reason with the highest baseline of all), the FWHM does increase with density. This indicates a decrease of T_2 relative to bulk with increasing ρ. Such dependence could be interpreted as evidence for the increasingly glassylike behavior of the 8CB molecules, with no obvious differences between the nematic and smectic phases. This, in turn, suggests that the glassy characteristics are unaffected by smectic ordering. Still, direct NMR measurements of T_2 would be extremely valuable and conclusive.

IV. CONCLUSIONS

We have presented DNMR results for 8CB confined to silica aerogel. This investigation was systematically performed as a function of aerogel density and temperature spanning the isotropic, nematic, and smectic-A phases. The quenched disorder introduced by the host aerogel drastically alters the phase and orientational behavior of the liquid-crystal material.

In the isotropic phase, there is remnant surface-induced (paranematic) order. This ordering, due to the silica surfaces, is reflected as a single but broader than bulk absorption peak. The FWHM of this peak increases with aerogel density, indicating that surface effects become stronger in higher density aerogel (or equivalently more restrictive pore size) due to the increase in available surface area. The manner in which the FWHM grows with decreasing temperature appears as quasicomplete wetting of the silica surface by the nematic phase. This suggests perpendicular anchoring of the director at the silica surface.

The orientational order in the nematic phase is characterized by powder-pattern DNMR spectra for all densities but the highest. This is representative of the presence of nematic domains randomly oriented, disordered by the isotropic structure of the random host. More importantly, these domains seem to be characterized by a single value of orientational order Q, although there may be some small variations, especially near the silica surface. In addition, this suggests that for $\rho<\rho_C\approx 0.5\,\mathrm{g/cm}^3$, the nematic ordering is defect-free. For $\rho>\rho_C$, as in the case of Vycor glass, a single absorption peak whose width continuously increases with decreasing temperature is found. In addition to a random $\hat{n}$, there exists a broad distribution of Q and, likely, the presence of defects.

With increasing aerogel density, the weakly first-order nematic-to-isotropic phase transition becomes gradual; it is eventually replaced with a continuous evolution of orientational order. The enhancement of orientational order that occurs at the bulk smectic-A to nematic transition is not seen under confinement. Since in this range of aerogel density x-ray studies find smectic scattering, this indicates a confinement-induced decoupling of smectic and nematic order parameters. Further, it was empirically found that the behavior of the FWHM of the nematic powder-pattern singularities as a function of temperature is similar to that of the specific heat: with decreasing L, the SmA-N transition is highly suppressed and, finally, completely eliminated. This is suggestive of glassy dynamics, which do not appear to differ

between the nematic and smectic phases in aerogel. Nevertheless, it would be valuable to perform NMR measurements of the T_2 relaxation.

In closing, it is worthwhile to discuss our present observations in light of the very recent theoretical efforts of Radzihovsky, Toner, and co-workers (RT), in which they explored the stability and phase behavior of smectics confined to aerogel [13]. For sufficiently weak disorder, they predict the replacement of the bulk Sm*A*-*N* transition with a transition from a nematic-elastic glass (NEG) to a smectic-Bragg glass (SmBG-NEG). The characteristics of these new phases are long-range orientational order, glassy dynamics, and the presence of defects, specifically dislocation loops. In this scenario, the SmBG-NEG is mediated by a defect unbinding mechanism. Our study cannot address the length scale of $\vec{Q}$ directly. In addition, given the recent light-scattering analysis, the director is randomized on quasi-long-range scales. Here, although we find evidence of glassy behavior, it appears to be the same in the smectic and nematic phases; this argues against a defect unbinding mechanism. For the aerogel low density samples (close to the weak disorder limit of RT), the observed powder patterns suggest a highly distorted but defect-free nematic structure. Further theoretical and experimental studies would still be welcome.

ACKNOWLEDGMENTS

This research was supported by the NSF-STC ALCOM DMR Grant No. 89-20147. We are indebted to Professor Carl Garland for many illuminating conversations and constant encouragement to write these results, and to Professor Noel Clark and Professor Slobodan Zumer, with whom we have had several stimulating discussions. We are extremely grateful to Mary Neubert and her co-workers whom, through the Resource Facility of ALCOM, provided us with the deuterated 8CB.

[1] F. M. Gasparini and I. Rhee, in *Progress in Low Temperature Physics*, edited by D. F. Brewer (North-Holland, Amsterdam, 1992), Vol. XIII, Chap. 1.

[2] D. Finotello, K. A. Gillis, A. Wong, and M. H. W. Chan, Phys. Rev. Lett. **61**, 1954 (1988); M. H. W. Chan, K. I. Blum, S. Q. Murphy, G. K. S. Wong, and J. D. Reppy, *ibid.* **61**, 1950 (1988).

[3] M. H. W. Chan, N. Mulders, and J. D. Reppy, Phys. Today **49**(8), 30 (1996).

[4] M. C. Goh, W. I. Goldburg, and C. M. Knobler, Phys. Rev. Lett. **58**, 1008 (1987).

[5] S. B. Dierker and P. Wiltzius, Phys. Rev. Lett. **58**, 1865 (1987); **66**, 1185 (1991); P. Wiltzius, S. B. Dierker, and B. S. Dennis, *ibid.* **62**, 804 (1989); S. B. Dierker, B. S. Dennis, and P. Wiltzius, J. Chem. Phys. **92**, 1320 (1992).

[6] F. Brochard and P. G. de Gennes, J. Phys.(France) Lett. **44**, 785 (1983); P. G. de Gennes, J. Phys. Chem. **88**, 6469 (1984), and references therein.

[7] X-l. Wu, W. I. Goldburg, M. X. Liu, and J. Z. Xue, Phys. Rev. Lett. **69**, 470 (1992).

[8] T. Bellini, *et al.*, Phys. Rev. Lett. **69**, 788 (1992); N. A. Clark *et al.*, *ibid.* **71**, 3505 (1993); T. Bellini, N. A. Clark, and D. W. Schaefer, *ibid.* **74**, 2740 (1995); T. Bellini, N. A. Clark, V. Degiorgio, F. Mantegazza, and G. Natale, Phys. Rev. E **57**, 2996 (1998).

[9] L. Wu, B. Zhou, C. W. Garland, T. Bellini, and D. W. Schaefer, Phys. Rev. E **51**, 2157 (1995); B. Zhou, G. S. Iannacchione, C. W. Garland, and T. Bellini, *ibid.* **55**, 2962 (1997).

[10] S. Qian, G. S. Iannacchione, and D. Finotello, Phys. Rev. E **53**, R4291 (1996); **57**, 4305 (1998).

[11] A. Maritan, M. Cieplak, T. Bellini, and J. R. Banavar, Phys. Rev. Lett. **72**, 4113 (1994); A. Maritan, M. Cieplak, and J. R. Banavar, in *Liquid Crystals in Complex Geometries Formed by Polymer and Porous Networks*, edited by G. P. Crawford and S. Zumer (Taylor and Francis, London, 1996), Chap. 22.

[12] D. J. Cleaver, S. Kralj, T. J. Sluckin, and M. P. Allen, in *Liquid Crystals in Complex Geometries Formed by Polymer and Porous Networks* (Ref. [11]), Chap. 21.

[13] L. Radzihovsky and J. Toner, Phys. Rev. Lett. **78**, 4414 (1997); **79**, 4214 (1997); Phys. Rev. B **60**, 206 (1999).

[14] A. J. Liu *et al.*, Phys. Rev. Lett. **65**, 1897 (1990); A. J. Liu and G. S. Grest, Phys. Rev. A **44**, R7894 (1991); L. Monette, A. J. Liu, and G. S. Grest, *ibid.* **46**, 7664 (1992).

[15] F. Aliev, W. I. Goldburg, and X-l. Wu, Phys. Rev. E **47**, R3834 (1993); W. I. Goldburg, F. M. Aliev, and X-l. Wu, Physica A **213**, 61 (1995).

[16] S. Kralj, G. Lahajnar, A. Zidansek, N. Vrbancic-Kopac, M. Vilfan, R. Blinc, and M. Kosec, Phys. Rev. E **48**, 340 (1993).

[17] G. S. Iannacchione *et al.*, Phys. Rev. Lett. **71**, 2595 (1993); Mol. Cryst. Liq. Cryst. Sci. Technol., Sect. A **262**, 13 (1995); Phys. Rev. E **53**, 2402 (1996).

[18] G. Iannacchione and D. Finotello, in *Liquid Crystals in Complex Geometries Formed by Polymer and Porous Networks* (Ref. [11]), Chap. 16.

[19] Z. Zhang and A. Chakrabarti, Phys. Rev. E **52**, 4991 (1995).

[20] D. W. Schaefer and K. D. Keefer, Phys. Rev. Lett. **56**, 2199 (1986); F. Ferri, B. J. Frisken, and D. S. Cannell, *ibid.* **67**, 3626 (1991).

[21] G. S. Iannacchione, C. W. Garland, J. T. Mang, and T. P. Rieker, Phys. Rev. E **58**, 5966 (1998).

[22] A. Zidansek, S. Kralj, G. Lahajnar, and R. Blinc, Phys. Rev. E **51**, 3332 (1995).

[23] 8CB was synthesized and deuterated in the ALCOM resource facility.

[24] M. Hara, Y. Iwakabe, K. Tochigi, H. Sasabe, A. F. Garito, and A. Yamada, Nature (London) **344**, 228 (1990).

[25] J. Thoen, H. Marynissen, and W. Van Dael, Phys. Rev. A **26**, 2886 (1982); C. W. Garland, in *Phase Transitions in Liquid Crystals*, edited by S. Martellucci and A. N. Chester (Plenum, New York, 1992).

[26] J. W. Doane, in *Magnetic Resonance of Phase Transitions*, edited by F. J. Owens, C. P. Poole, and H. A. Farach (Academic, New York, 1979); P. Ukleja and D. Finotello, Techniques in Liquid Crystals, edited by S. Kumar (Cambridge University Press, Cambridge, in press), Chap. 5.

[27] G. P. Crawford and J. W. Doane, Mod. Phys. Lett. B **28**, 1785 (1993), and references therein.

[28] S. Kralj, A. Zidansek, G. Lahajnar, S. Zumer, and R. Blinc, Phys. Rev. E **57**, 3021 (1998).

[29] H. Zeng and D. Finotello, Phys. Rev. Lett. **81**, 2703 (1998).

[30] M. Vilfan and N. Vrbancic-Kopac, in *Liquid Crystals in Complex Geometries Formed by Polymer and Porous Networks* (Ref. [11]), Chap. 7.
[31] S. Zumer, S. Kralj, and M. Vilfan, J. Chem. Phys. **91**, 6411 (1989).
[32] P. G. de Gennes, *The Physics of Liquid Crystals* (Clarendon, Oxford, 1974).
[33] G. P. Crawford, R. Stannarius, and J. W. Doane, Phys. Rev. A **44**, 2558 (1991).
[34] G. S. Iannacchione, S. Qian, D. Finotello, and F. Aliev, Phys. Rev. E **56**, 554 (1997).
[35] J. Dolinsek, O. Jarh, M. Vilfan, S. Zumer, R. Blinc, J. W. Doane, and G. P. Crawford, J. Chem. Phys. **95**, 2154 (1991).
[36] G. P. Crawford, R. J. Ondris-Crawford, J. W. Doane, and S. Zumer, Phys. Rev. E **53**, 3647 (1996), and references therein.
[37] B. Jerome, Rep. Prog. Phys. **54**, 391 (1991).
[38] A. Mertelj and M. Copic, Phys. Rev. E **55**, 504 (1997).
[39] A. Golemme, S. Zumer, D. W. Allender, and J. W. Doane, Phys. Rev. Lett. **61**, 2937 (1988).
[40] Numerical simulations of DNMR spectral patterns as they become affected by different translational diffusion rates can be found in Ref. [15].
[41] M. Vilfan, N. Vrbancic-Kopac, B. Zalar, S. Zumer, and G. P. Crawford, Phys. Rev. E **59**, R4754 (1999).